Sensors and Actuators A 294 (2019) 61–72

Contents lists available at ScienceDirect

Sensors and Actuators A: Physical

journal homepage: www.elsevier.com/locate/sna

A high energy dielectric-elastomer-amplified piezoelectric (DEAmP) to harvest low frequency motions

Anup Teejo Mathew, Chong Liu, Tian Yao Nicholas Ng, Soo Jin Adrian Koh*

Department of Mechanical Engineering, National University of Singapore, 9 Engineering Drive 1, Singapore, 117575, Singapore

ARTICLE INFO

Article history:
Received 21 January 2019
Received in revised form 28 March 2019
Accepted 11 May 2019
Available online 12 May 2019

Keywords:
Dielectric elastomer
Energy harvesting
Hybrid generator
Piezoelectric

ABSTRACT

A dielectric elastomer generator (DEG) needs a high voltage priming source and large operating strains to produce a specific energy output in excess of 1 J/kg. For small-scale energy harvesting applications like a heel-strike generator, there is limited space. Providing such a priming source and a large amount of strain in a constrained space is challenging. To address this challenge, we present a dielectric-elastomer-amplified piezoelectric (DEAmP) generator. The piezoelectric generator charges the DEG and the DEG amplifies the voltage of the charges placed on it. Using a piezoelectric as a priming source makes our system much more compact and autonomous than others that use batteries and amplifiers as priming sources. From analysis, we define conditions of operation where there is a net amplification by the DEG and identify optimal conditions where up to 250 times in amplification of output energy could be produced. To produce large deformation on the DE within a constrained space, we propose the ripple mode of deformation. A simple analytical model and a design plot of the ripple mode was presented. Following our analyses, we construct a 3D-printed prototype that would demonstrate gain in energy harvested from a generic source of motion, reminiscent to that of a human footfall. We showed that the piezoelectric generator used in our experiment singly produces a specific energy output of 0.16 mJ/g, whereas the DEAmP generator yields 0.29 mJ/g. We showed the capability of a DEAmP to deliver an amplified output as compared to a standalone piezoelectric, even when harvesting low frequency motions. We discuss several strategies to further enhance the performance of a DEAmP.

1. Introduction

Harvesting ambient energy presents an attractive proposition in the field of renewable energy as it is freely available and pervasive. This study focuses on energy harvesting of a particular type – ambient motion. Ambient motion has been traditionally harvested in its high speed forms, by electromagnetic generators and piezoelectrics [1]. The need for high speed excitations stems from the low energy density of such systems, calling for the need to absorb ambient energy at a rapid rate, so as to produce sufficient power yield [2]. Hence, harvesting ambient motion is often termed "kinetic energy harvesting". Low frequency motions have been conspicuously challenging to harvest. One striking example is harvesting wave motions, which has seen limited success due to the need to translate low-frequency source motion to a high-frequency input into conventional energy converters such as piezoelectric or electromagnetic generators [3,4]. Energy harvesters harvest motions based primarily on three physical processes – electromagnetism, piezoelectricity and electrostatics [2,5,6]. Currently, electromagnetic generators are the only energy harvesting technology that is deployed on a large-scale basis. The others remain active research topics that find themselves limited to laboratory testing and prototyping. A key limiting factor remains to be its very low energy density [5,7].

A dielectric elastomer generator (DEG) is an electrostatic generator that converts elastic energy to electrical energy via capacitance change due to mechanical deformation (Fig. 1a). When a low voltage charge is placed on a stretched elastomer prior to contraction, the contraction work against the Maxwell pressure increases the potential (voltage) of the charge, thus generating energy [2,7–10]. DEGs have been found, both theoretically and experimentally, to have specific energies of at least ten times that of existing technologies like piezoelectric and electromagnetics [5,7]. It is low cost, exhibits noise-free operation, excellent resistance to corrosion and has good impedance matching to many energy sources [8,11–13]. Specific energy and conversion efficiency of up to 0.78 J/g and 30% are reported for an equal-biaxial DEG using a high voltage electrical source [14]. DE transducers were recently identified as a promis-

* Corresponding author.
E-mail address: adrian_koh@nus.edu.sg (S.J.A. Koh).

https://doi.org/10.1016/j.sna.2019.05.015
0924-4247/

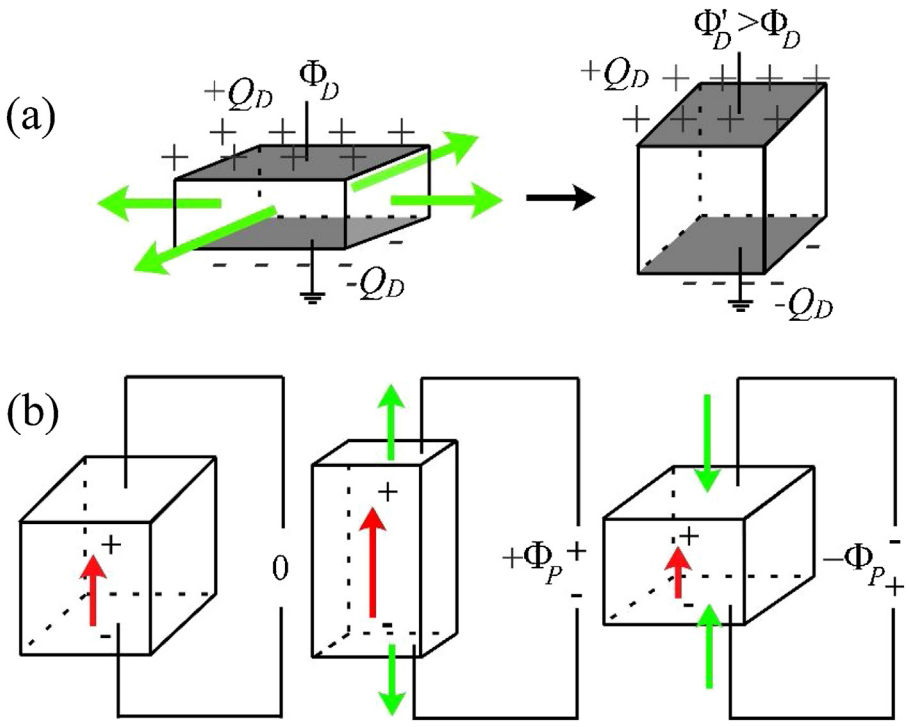

Fig. 1. (a) Dielectric elastomer generator: A dielectric elastomer is sandwiched between compliant electrodes (grey color). The electric potential of charges placed on a DEG prior to contraction, increases due to the contraction work done against the electrostatic (Maxwell) pressure. (b) Piezoelectric generator: Piezoelectric materials have a non-symmetric crystal structure. Under the influence of an external force (tension or compression) the polarization inside a piezoelectric material changes, resulting in voltage/charge generation. Voltage and charge are represented using symbols, Φ and Q. Subscripts "D" and "P" indicate DEG and piezoelectric generator respectively. Green arrows show the direction of force and the red arrows show the polarization of the piezoelectric. (For interpretation of the references to colour in this figure legend, the reader is referred to the web version of this article).

ing technology for the marine energy sector to harvest sea waves [15,16]. However, DEG requires an external high voltage power source such as a battery as its priming source. Operating strains of a DEG are typically high [17–20], making it challenging to devise a compact design. These two factors combine to present a challenge for widespread development, investigation and adoption of this technology.

There are previous attempts on making DEG autonomous and compact that is free from the need to tether it to an external high voltage electrical source. For instance, Mistral et. al, coupled the dielectric elastomer with an electret [21–24]. With an electret material charged to -1000 V an experimental specific energy of 0.55 mJ/g is demonstrated for a hybrid electret-DEG working in electret mode [23]. However, the specific energy of the electret used for the experiment was not provided for the comparison of the energy amplification. Electrets are readily available and are expensive to purchase or produce. They require periodic priming from plasma discharge as its charges will eventually be depleted. Anderson et al., proposed a self-priming circuit with microbial fuel cells (MFCs) or solar cell arrays as the initial priming source [25–27]. The self-primed DEG demonstrated a specific energy of up to 10 mJ/g while boosting the voltage from a 10 V to 2000 V in about 30 cycles [28]. MFCs or solar cell arrays may present integration problems to DEG as their physical process of energy conversion are dissimilar to DEGs. The self-primed DEG also requires a number of cycles to increase its low voltage into a desirable range ($\tilde{1}$000 V). For a low-frequency sporadic mechanical source, excessive charge leakage may greatly compromise on the effectiveness of voltage boost.

We investigate a piezoelectric diaphragm as a priming source for the DEG. When a piezoelectric material is mechanically deformed, its non-symmetrical crystalline structure will be electrically polarized due to the mechanical deformation (Fig. 1b). The resulting charge/voltage generation will be used to prime the DEG. The DEG will then amplify this input energy via voltage boost, thereby yielding a higher output. We name the generator a *dielectric-elastomer-amplified piezoelectric* (DEAmP) generator. Alexandru et al. and Lagomarsini et al. have used a piezoelectric generator as the priming source for a DEG [29,30]. Alexandru et al. demonstrated an energy output of 2.13 μW under 50% strain at 1 Hz for a piezoelectric generator that generates a priming voltage of 180 V. They also estimate a specific power of 285 μW/g for a DEG operating in 100% strain under a bias voltage of 1 kV from a piezoelectric element. Lamgomarsini et al. demonstrated up to 14.3 μJ/g for a PZT-DEG hybrid generator. However, in both the works, the capacitance change of the DEG may not be enough to ensure an effective energy amplification for the hybrid generator compared to a standalone piezoelectric. We provide a comprehensive analysis of a single cycle of the hybrid generator to choose the required operational parameters for the DEG that ensures an effective energy amplification. We further propose a simple way to induce large capacitance change within a constrained space and integrate the piezoelectric and the dielectric elastomer film so that a single compressive load provides the optimal operation of the hybrid generator prototype.

Depending on the vibration source, piezoelectric generators are operated at low to high frequencies (Hz to kHz) [31–33]. Here, we perform a quasi-static deformation of a piezoelectric generator operating at a low frequency (around 1 Hz), so as to sync it with the deformation period of the DEG and the low frequency motion source. Based on a simplified circuit of the piezoelectric generator operating in a low frequency, we develop an analytical model to find the energy yield of the hybrid generator. We compared the energy yield with the maximum energy output of a single piezoelectric generator across a resistive load. The analysis revealed conditions under which there is a net gain in energy output when the DEG

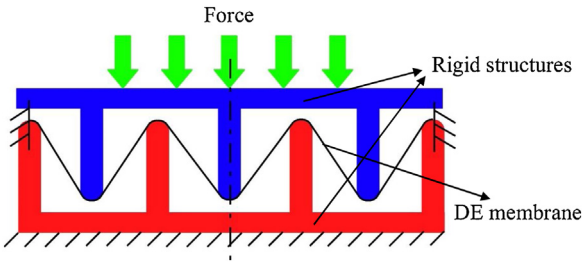

Fig. 2. Cross-sectional view of *ripple* configuration of DE. The rigid structures deform a circular diaphragm type DE into out-of-plane direction resulting in a shape similar to ripples in water.

is coupled with the piezoelectric. We designed our experimental prototype based on our analysis.

The high energy density of DEG is attributed solely to its ability to undergo large elastic deformation. Large elastic deformation induces a very large capacitance change [19]. Often DEGs must be deformed to strains beyond 100% in order to produce outputs that surpasses existing technologies [18]. We present a simple mode of deformation that is capable to deform a DE to a large strain within a small space, which we term the *ripple* (Fig. 2). We used geometrical analysis to obtain the deformed stretch and capacitance of the configuration. We follow with a design plot to aid in the selection of design parameters for the construction of the *ripple*.

Finally, we construct a prototype using the design parameters suggested by our analysis. We conducted an experimental characterization to measure the electrical output of the piezoelectric operating singly, and the DEG coupled with the piezoelectric. Our analysis presented good agreement with our experimental results, and the energy amplification was clearly demonstrated due to the coupling of DEG with a piezoelectric. In the concluding section, we discuss strategies to further improve the energy output.

2. Analysis of DEAmP

Prior to analysing the energy output of the hybrid DEAmP generator we derive the maximum energy output of a piezoelectric generator across a resistive load. Later we use this as a basis to compare the energy output of the hybrid generator.

2.1. Piezoelectric generator

We first analyse a piezoelectric generator. A piezoelectric generator can be represented as Norton or Thevenin equivalent circuits as shown in Fig. 3a and Fig. 3b. The current source, i_{SC} in Fig. 3a is the short-circuit output current, and the voltage source, Φ_{OC} in Fig. 3b is the open-circuit output voltage [34]. Z_P represents the internal impedance of the piezoelectric. As our system involves current of very small magnitudes (in μA to mA) and a very high voltage (10^2 V), we adopt the Thevenin equivalent for our analysis. Generally, the impedance, Z_P is represented using Van Dyke model as shown in Fig. 3c [34–36]. The Van Dyke model is a parallel connection of an LCR circuit as equivalent circuit components representing the mechanical inertia, stiffness and damping of the piezoelectric material, with a capacitance representing the electrostatic capacitance of the piezoelectric layer, C_P. In low frequency/off resonance operation, the rate of change of current is low. Hence we neglect the inductive component of the Van Dyke model to simplify it as shown in Fig. 3d [37,38].

The value of piezoelectric capacitance C_P and R_P can be determined by using an impedance analyzer [38]. For an ideal piezoelectric model, the internal resistance R_P is equal to zero [39]. Hence, for our analysis we consider the piezoelectric impedance purely as a capacitive system. The open-circuit voltage of the piezoelectric depends on the dynamics of the force application. For a compression force we model the piezoelectric open-circuit voltage as a ramped pulse as shown in Fig. 4a [40]. The actual values of Φ_{P_MAX}, t_a, t_b and t_c depend on the way of application of the force on the piezoelectric. From time 0 to t_a the applied force increases, from t_a to t_b the force is held constant and from t_b to t_c the force is released. For simplicity, we linearize all processes.

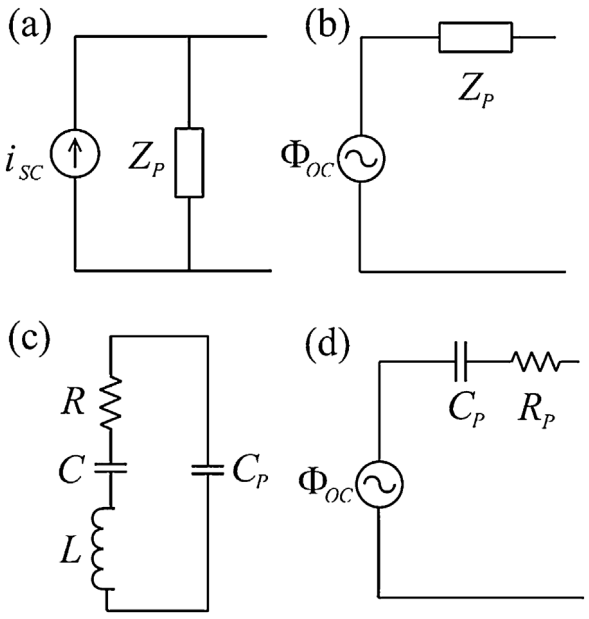

Fig. 3. (a) Norton equivalent of the piezoelectric generator (b) Thevenin equivalent of the same. (c) Equivalent internal impedance of the piezoelectric generator. (d) Off-resonance model of the piezoelectric generator.

Based on the open-circuit voltage profile we obtain the output voltage on any electrical load connected in parallel with the piezoelectric [40]. A typical voltage profile across a resistive load while the piezoelectric is deformed is given in Fig. 4b. For an electric load with infinite resistance the output voltage follows same as the open-circuit voltage. In that case the charge transferred is zero. Similarly, for an electric load with zero resistance (short circuit condition) we have the maximum charge transfer, but the output voltage is zero in that case. Hence there exists a load resistance at which the maximum energy transfer happens, as denoted by the shaded area of Fig. 4c, which shows the voltage and charge relationship for a typical linear transducer. Due to linearity of voltage and charge, the maximum energy output occurs when the transducer voltage is half of its open-circuit voltage and the charge transferred is the half of its short circuit charge, as follows: $\Omega_{MAX} = \Phi_{OC} Q_{SC}/4$ [1]. Assuming that, Φ_{P_MAX} is the peak open-circuit voltage and $2Q_{P\_MAX}$ is the charge transferred in short circuit condition (the factor "2" is due to the positive and negative phases of the piezoelectric as shown in Fig. 4b), the maximum energy output of the piezoelectric generator is derived as:

$$\Omega_{P\_MAX} = \frac{1}{2}\Phi_{P\_MAX} Q_{P\_MAX} \tag{1}$$

Using the constitutive equations of a piezoelectric element [41], we write:

$$Q_{P\_MAX} = C_P \Phi_{P\_MAX} \tag{2}$$

Putting (2) in (1), we will have:

$$\Omega_{P\_MAX} = \frac{1}{2} C_P \Phi_{P\_MAX}^2 \tag{3}$$

which is a typical output energy equation for a capacitor.

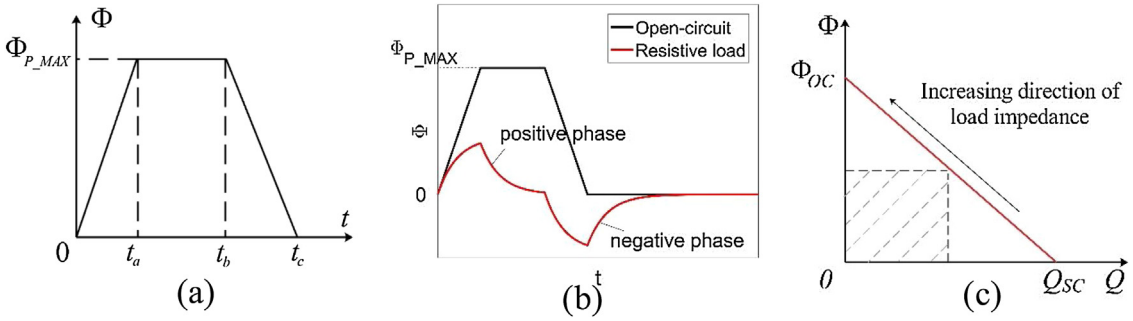

Fig. 4. (a) Open circuit voltage of the piezoelectric generator. (b) A typical piezoelectric voltage profile across a resistive load. The positive and negative phases for a resistive load are due to the change in direction of current through it (c) Voltage and charge relationship for a typical linear transducer for various load impedance. Φ_{OC} is the open circuit voltage and Q_{SC} is the charge transferred in the short circuit condition.

2.2. DEAmP generator

Fig. 5a show one of the simplest energy harvesting circuits using a DE generator (DEG). A DEG is a variable capacitor with capacitance C_D. The voltage Φ_D and the charges Q_D on a DEG will vary with its capacitance as follows:

$$Q_D = C_D \Phi_D \tag{4}$$

and that:

$$C_D = \frac{\varepsilon_0 \varepsilon_r a}{h} \tag{5}$$

where, ε_0 is the permittivity of free space, ε_r is the relative permittivity of the dielectric, a is the deformed area and h is the deformed thickness. Eqs. (4) and (5) suggest that the capacitance is a variable that depends on the state of deformation. The DE follows the cycle of operation described in Fig. 5c. For 1→2, the uncharged DEG is stretched in open-circuit condition. Stretching increases the area and decreases the thickness of the DE membrane. Hence, from Eq. (5), the capacitance of the DEG is increased. At state 2, DEG attains its highest capacitance, C_{D_MAX}. For 2→3, the DEG is connected to the voltage source via a switch. The DEG gets charged at a fixed stretch ($C_D = C_{D\_MAX}$) until it equilibrates with the electrical potential of the source. For 3→4, the DEG is relaxed in open-circuit condition so that its capacitance drops from its maximum value to its minimum value, C_{D_MIN}. From Eq. (4), mechanically relaxing the DE in open-circuit will cause the voltage across its electrodes to increase. At maximum voltage state 4, the DEG will be discharged at fixed stretch ($C_D = C_{D\_MIN}$) through a drain resistor. We replace the voltage source in Fig. 5a with a piezoelectric generator with a full wave bridge rectifier, as shown in Fig. 5b. The piezoelectric generator will be deformed to charge the DEG at state 2→3. To simplify our analysis, we assume a fixed state of deformation when the DE is charged (2→3) and discharged (4→1).

For state 1→2, the DE is stretched from C_{D_MIN} to C_{D_MAX}:

$$\Phi_{D(1\to2)} = 0 \tag{6a}$$

$$Q_{D(1\to2)} = 0 \tag{6b}$$

For state 2→3, the piezoelectric generator is deformed, and the DEG gets charged. The DEG is charged by a piezoelectric while it is at its maximum capacitance. From Eq. (4) we have:

$$Q_{D(2\to3)} = C_{D\_MAX} \Phi_{D(2\to3)} \tag{7}$$

The equivalent circuit for this charging process is given in Fig. 6. The entire charging process consists of two time periods based on the open-circuit voltage time-history of the piezoelectric given in Fig. 4a. During the first time period, that is from 0 and t_b, the DEG (C_{D_MAX}) and the piezoelectric capacitor (C_P) gets charged. The peak piezoelectric open-circuit voltage (Φ_{P_MAX}) gets divided across the DEG and the piezoelectric capacitor as shown in Fig. 6a. The second time period is when $t > t_b$. In this period, if $C_{D\_MAX} < C_P$, then the voltage across the DEG is larger than the voltage across the piezoelectric capacitor. Hence there will not be any charge transfer and capacitors C_{D_MAX} and C_P remain in a state of voltage equilibrium due to the reverse-biased diodes. However, if $C_{D\_MAX} \geq C_P$, charge will be transferred from the piezoelectric to the DEG, until a new equilibrium is attained, as shown in Fig. 6b, with its value as follows:

$$\Phi_{eq} = \frac{2C_P C_{D\_MAX}}{(C_P + C_{D\_MAX})^2} \Phi_{P\_MAX} \tag{8a}$$

Hence the voltage on DEG at state 3 can be derived as:

$$\Phi_{D3} = \begin{cases} \dfrac{C_P}{C_P + C_{D\_MAX}} \Phi_{P\_MAX} \text{ if } C_{D\_MAX} < C_P \\ \dfrac{2C_P C_{D\_MAX}}{(C_P + C_{D\_MAX})^2} \Phi_{P\_MAX} \text{ if } C_{D\_MAX} \geq C_P \end{cases} \tag{8b}$$

We assume that, compared to the priming voltage of the DEG (>100 V for our prototype), voltage drop across the diodes of the bridge rectifier is negligible. Using the equation for energy stored in a capacitor ($C\Phi^2/2$), the total energy transferred to the DEG can be calculated as:

$$\Omega_{D\_in} = \begin{cases} \dfrac{1}{2} C_{D\_MAX} \left(\Phi_{P\_MAX} \dfrac{C_P}{C_P + C_{D\_MAX}} \right)^2 \text{ if } C_{D\_MAX} < C_P \\ \dfrac{1}{2} C_{D\_MAX} \left(\Phi_{P\_MAX} \dfrac{2C_P C_{D\_MAX}}{(C_P + C_{D\_MAX})^2} \right)^2 \text{ if } C_{D\_MAX} \geq C_P \end{cases} \tag{9a}$$

We define the energy retained within the piezoelectric as:

$$\Omega_{P\_r} = \begin{cases} \dfrac{1}{2} C_P \left(\Phi_{P\_MAX} \dfrac{C_{D\_MAX}}{C_P + C_{D\_MAX}} \right)^2 \text{ if } C_{D\_MAX} < C_P \\ \dfrac{1}{2} C_P \left(\Phi_{P\_MAX} \dfrac{2C_P C_{D\_MAX}}{(C_P + C_{D\_MAX})^2} \right)^2 \text{ if } C_{D\_MAX} \geq C_P \end{cases} \tag{9b}$$

For state 3→4, the DE is relaxed from C_{D_MAX} to C_{D_MIN} in open-circuit:

$$\Phi_{D(3\to4)} = \frac{C_{D\_MAX}}{C_D} \Phi_{D3} \tag{10a}$$

$$Q_{D(3\to4)} = C_{D\_MAX} \Phi_{D3} \tag{10b}$$

$$\Phi_{D4} = \frac{C_{D\_MAX}}{C_{D\_MIN}} \Phi_{D3} \tag{10c}$$

For state 4→1, the energy stored in the DEG gets discharged. The DEG is discharged in its minimum capacitance state. Hence,

$$Q_{D(4\to1)} = C_{D\_MIN} \Phi_{D(4\to1)} \tag{11a}$$

$$\Phi_{D1} = 0 \tag{11b}$$

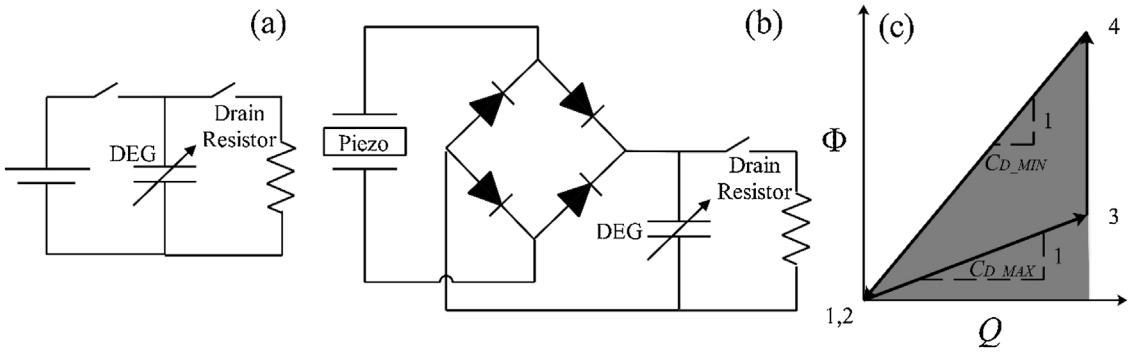

Fig. 5. (a) Energy harvesting circuit of a DEG primed by a high voltage source. (b) Modified circuit by replacing the priming source with a piezoelectric generator and a bridge rectifier. (c) DEG cycle in the voltage charge plane. The shaded area represents the energy output from DEG.

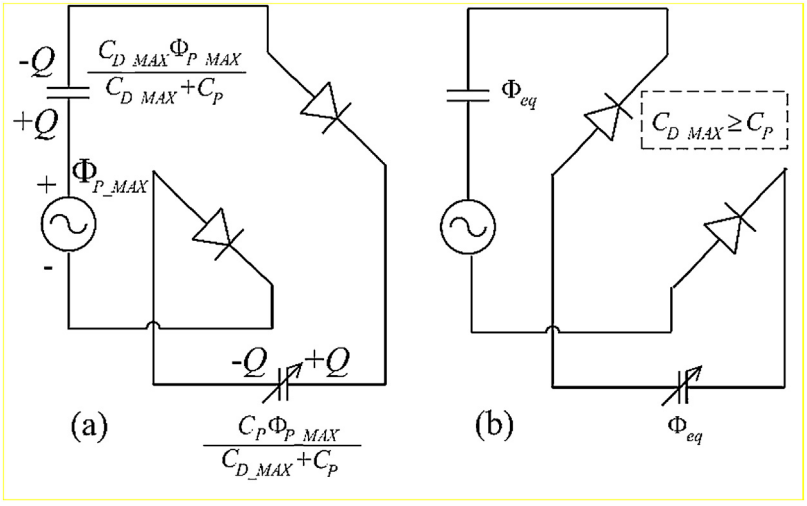

Fig. 6. Equivalent circuit of a piezoelectric element charging a DEG. (a) Part 1: during time 0 to t_b (b) Part 2: during $t > t_b$.

Applying capacitance energy equation at state 4, the total energy output (discharged) from the DEG can be calculated as:

$$\Omega_{D\_out} = \begin{cases} \frac{1}{2}C_{D\_MAX}\left(\Phi_{P\_MAX}\frac{C_P}{C_P+C_{D\_MAX}}\right)^2\frac{C_{D\_MAX}}{C_{D\_MIN}} \text{ if } C_{D\_MAX} < C_P \\ \frac{1}{2}C_{D\_MAX}\left(\Phi_{P\_MAX}\frac{2C_PC_{D\_MAX}}{(C_P+C_{D\_MAX})^2}\right)^2\frac{C_{D\_MAX}}{C_{D\_MIN}} \text{ if } C_{D\_MAX} \geq C_P \end{cases} \quad (12)$$

As the DEG and the piezoelectric are connected in parallel with the drain resistor during the process (Fig. 5b), the energy retained within the piezoelectric capacitor will also get discharged. Hence the total energy output of the DEAmP generator is the sum of energy output from DEG and the energy retained within the piezoelectric,

$$\Omega_{out} = \Omega_{D\_out} + \Omega_{P\_r} \quad (13)$$

We define β as the ratio of maximum and minimum capacitance of DEG: $\beta = C_{D\_MAX}/C_{D\_MIN}$ and γ as the ratio of minimum capacitance of DEG and the capacitance of piezoelectric: $\gamma = \frac{C_{D\_MIN}}{C_P}$.Using Eqs. (3),(9b), (12) and (13) we write:

$$\frac{\Omega_{out}}{\Omega_{P\_MAX}} = \begin{cases} \left(\frac{\beta\gamma}{1+\beta\gamma}\right)^2 + \beta^2\gamma\left(\frac{1}{1+\beta\gamma}\right)^2 \text{ if } \beta\gamma < 1 \\ \left(\frac{2\beta\gamma}{(1+\beta\gamma)^2}\right)^2 + \beta^2\gamma\left(\frac{2\beta\gamma}{(1+\beta\gamma)^2}\right)^2 \text{ if } \beta\gamma \geq 1 \end{cases} \quad (14)$$

There will be charge leakage through the DE membrane and in the electric circuit resulting in a lower energy amplification. However, these effects are ignored in our analysis. Eq. (14) is represented as a design plot in Fig. 7. The capacitance ratio of a DEG is proportional to the power of stretch, λ^p (λ is the linear length ratio of deformed and undeformed state of the elastomer), where p is highest for the equal-biaxial mode of stretching ($p = 4$) [19,42]. For a common dielectric elastomer, VHB the maximum equal-biaxial stretch prior to mechanical rupture is around 5 [17]. Hence β is limited to 625 (5^4) in Fig. 7a. For a small scale DEG, due to the space constrain for deformation it may be challenging to achieve such large values of . Hence, we extract more practical values of β in the lower range, and plot them in Fig. 7b. Using Eq. (14) for a given, the optimum value of γ to have maximum energy amplification can be written as:

$$\gamma_{opt} = \frac{3\beta - 2 + \sqrt{(3\beta-2)^2 + 8\beta}}{2\beta^2} \quad (15)$$

Optimum value of γ is represented in Fig. 7. For known values of β and γ these plots can be used to evaluate the energy amplification of DEAmP generator. The values of β and γ for which the energy amplification of the hybrid generator is less than one, are represented as a black area. For this blacked-out region, it is more beneficial to use the piezoelectric generator in isolation than to couple it with a DEG. Fig. 7 shows that a high value of β and an optimum value of γ from Eq. (15) are desirable for the maximum energy amplification of the hybrid generator. For $\beta\tilde{6}25$, in ideal case it is possible to have an energy amplification as high as 250 times as shown in Fig. 7a. But practically this is limited by factors such

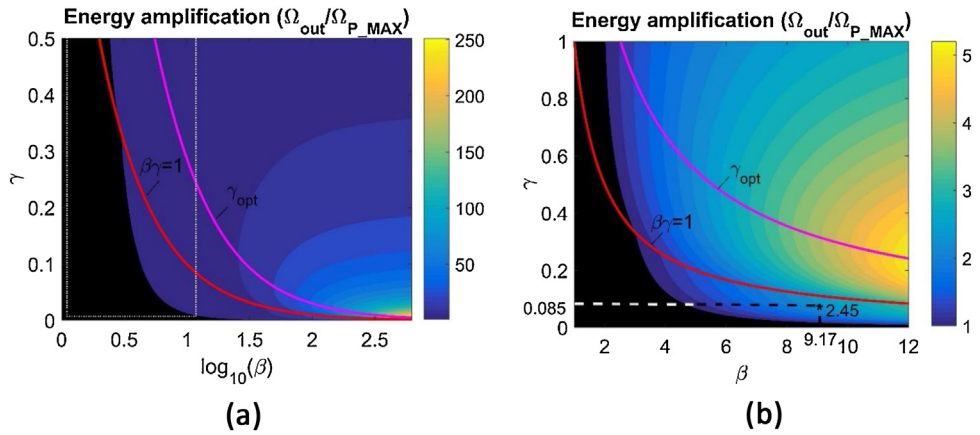

Fig. 7. (a) Design plot for choosing the values of β and γ for energy amplification. β varies from 1 to 625. (b) An area in (a) represented by a dotted rectangle is replotted for selecting the parameters for a small-scale DEG. The black region represents the values of β and γ for which the DEAmP will have a lower output energy compared to the piezoelectric generator. The dashed lines in (b) indicate the experimental conditions explained in a later section. $\beta = C_{D\_MAX}/C_{D\_MIN}$ and. $\gamma = C_{D\_MIN}/C_P$.

as the material limits of the elastomer used [17,43]. This point is discussed further in the Section 5 (Discussion).

3. DEAmP generator design

Fig. 7 suggests that the energy amplification of DEAmP generator increases with. Hence, the deformation of the DE should be made as large as possible. For small-scale energy harvesting applications like a heel-strike generator, several deformation modes such as fluid inflated diaphragm mode [2], stack design [44], DE diaphragm (loudspeaker) mode [26] are proposed. From geometry of the initial and deformed shape, the maximum β of a fluid inflated diaphragm mode of deformation can be estimated to be about 4. The practical values of β for the stack mode are typically low. For the diaphragm mode DE, a large value of β requires a large volume to deform, which makes it impractical for small-scale applications. Böse and Fuß introduced a sensor mat design to stretch the DE in a wave-like profile to enhance its sensitivity [45]. However, for this mode the capacitance change is not high, and the elastomer has open edges which affects its durability. We hereby introduce the *ripple* mode of deformation to achieve very large deformation within a constrained space without any free edges.

3.1. *The* ripple *mode*

Assuming a flat circular DE membrane deformed in the out-of-plane direction into a cone of height h_C, as shown in Fig. 8a in cross-sectional view. The capacitance of this configuration will scale approximately with h_C^2. But increasing h_C requires significant space to achieve large deformation. If we now make folds on this DE as shown in the second and third images of Fig. 8a, we will have the same amount of deformation on the membrane but requiring a much lesser space to deform. To realize such a deformation on a flat circular membrane, concentric rings of increasing diameter must be fashioned to create an interlocking system as shown in Fig. 8b. This mode of deformation, if looked from the top, resembles ripples on the surface of water (Fig. 8c). We hence term this mode of deformation the *ripple* mode. A pre-stretched flat circular membrane is fixed on a base structure (in red on Fig. 8b). An interlocking movable structure (in blue) is then used to deform the DE in the *ripple* mode. We define the *ripple* order n by the number of valley vertices (k), by $n = k-1$. Hence, from Fig. 8a, we have a zeroth, first and second order *ripple* from left to right. Assuming incompressibility of the dielectric elastomer [17,46] ($a \times h = V$ =constant, where V is the volume) in Eq. (5) we have:

$$C_D = \frac{\varepsilon_0 \varepsilon_r a^2}{V} \tag{16}$$

In Fig. 8b the deformed height of a n^{th} order *ripple* mode is h_R and its radius is r. This is equivalent to a cone of height h_C folded into a space of height h_R where, $h_R = h_C/(n+1)$. Hence the final area of the dielectric elastomer is given by the curved surface area of the cone, $a_f = \pi r\sqrt{r^2 + ((n+1)h_R)^2}$. Prior to deformation $h_R = 0$, recovering the area of a flat circle: $a_i = \pi r^2$. From Eq. (16), the capacitance ratio, C_{D_MAX}/C_{D_MIN} (β) can be derived as:

$$\beta = 1 + \left(\frac{(n+1)h_R}{r}\right)^2 \tag{17}$$

Like in the case of the diaphragm or loudspeaker-type DE [47], the *ripple* mode of deformation will exhibit some curvature instead of the linear profile of a cone. In our analysis we assume homogeneous deformation with no spatial variation in hoop stretch (λ_2). Hence, Eq. (17) provides an approximation to the actual capacitance ratio. Eq. (17) suggests a quadratic scaling of maximum capacitance change (β) with the product of *ripple* order (n+1) and the height aspect ratio (h_R/r). The maximum capacitance change, however, is further constrained by mechanical rupture of the elastomer [43,48,49]. Assuming Gaussian Chain statistics we impose a maximum value of $J = \lambda_1^2 + \lambda_1^2 + \lambda_1^{-2}\lambda_1^{-2} - 3$ as the rupture limit and term it as J_R [47].

$$J_R = \lambda_1^2 + \lambda_1^2 + \lambda_1^{-2}\lambda_1^{-2} - 3 \tag{18}$$

where J_R is 60 for VHB [47]. Let λ_1 be the radial stretch and λ_2 be the hoop stretch on an elastomer with a circular configuration. We assume a general case of an initial state of the elastomer, pre-stretched as a circular membrane on the rigid frame with equal-biaxial pre-stretch λ_p, we have:

$$\lambda_2 = \lambda_p \tag{19a}$$

As the flat circular membrane is deformed into a cone, we have:

$$\lambda_1 = \lambda_p \lambda_{1s} \tag{19b}$$

Where λ_{1s} is the ratio between the slanted length of the cone of the deformed membrane, and the original radius of the flat circular membrane. From geometry, we write:

$$\lambda_{1s} = \frac{a_f}{a_i} = \sqrt{1 + \left(\frac{(n+1)h_R}{r}\right)^2} = \sqrt{\beta} \tag{19c}$$

Putting (19a) and (19c) into (18), we have:

$$\lambda_p^2\beta + \lambda_p^2 + \lambda_p^{-4}\beta^{-1} - 3 = J_R \tag{20}$$

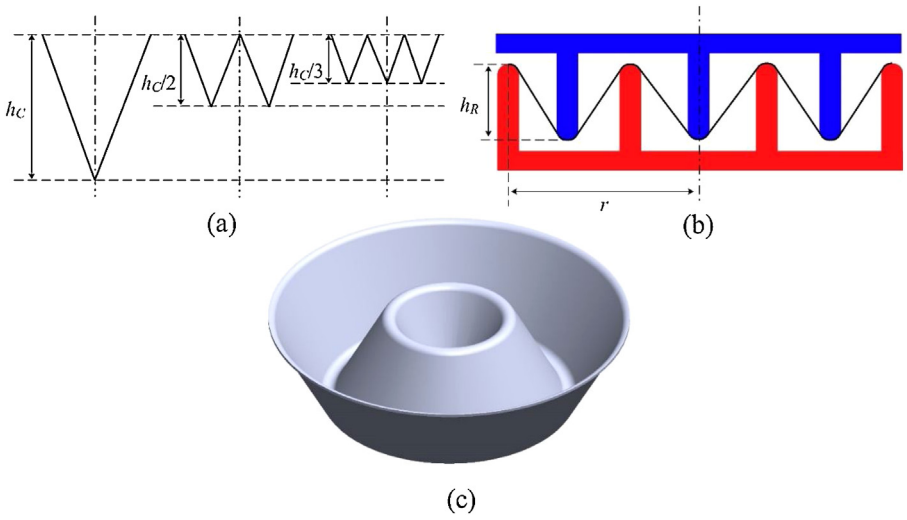

Fig. 8. (a) Concept of the *ripple* mode of deformation. (b) Realization of the 2nd order *ripple* (Axisymmetric-cross sectional view): The *ripple* mode of stretching of the elastomer is made possible by using the top (blue) and bottom (red) rigid structures. (c) 3D view of a DE deformed in second order *ripple* mode. (For interpretation of the references to colour in this figure legend, the reader is referred to the web version of this article).

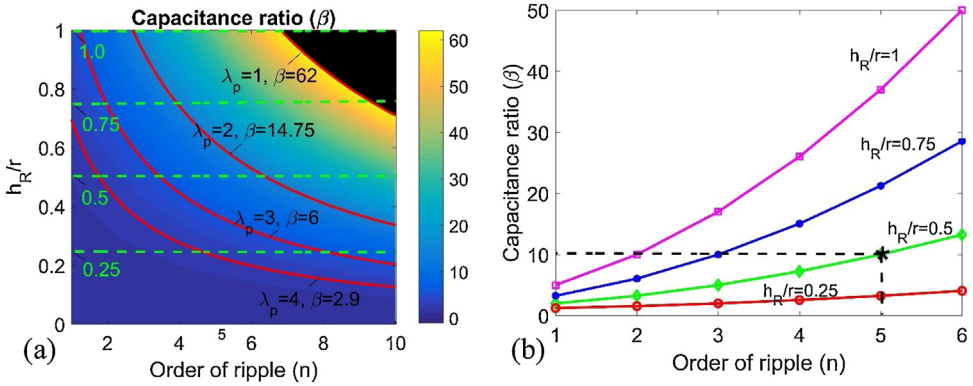

Fig. 9. (a) Design plot for the *ripple* mode based on Eq. (17). Red lines represent the rupture curve for a given equal-biaxial prestretch according to Eq. (20). The maximum capacitance ratios for a given pre-stretch are also indicated. The black region represents the region that are not admissible for the material with $J_R = 60$. (b) Capacitance ratio for four selected "h_R/r" shown as green dashed lines in (a). The black dashed lines indicate the *ripple* parameters used for the prototype fabrication. (For interpretation of the references to colour in this figure legend, the reader is referred to the web version of this article).

Fig. 9a illustrates Eq. (17) as a design plot, with the rupture limits (20) imposed as solid lines representing various levels of pre-stretch (λ_p). Fig. 9a serves to facilitate the selection of *ripple* order and the aspect ratio needed to achieve a desired deformation and thus capacitance change. The rupture criterion given in Eq. (20) is also shown in the figure. The value of J_R used is 60 [47]. For a better representation, four selected "h_R/r" ratios are plotted in Fig. 9b. The material thickness of the rigid *ripple* frame will also impose an additional constrain to the maximum number of ripples. One may not have an infinitely thin *ripple* frame as that will introduce stress concentration at the points of deformation. Later we use Fig. 9 together with Fig. 7 to check whether the chosen parameters for the prototype are within the admissible region. One should keep in mind that the rupture criterion used is solely based on the approximation of homogeneous deformation of the elastomer film. However, the *ripple* compression structure may introduce mechanical stress concentration points on the elastomer. As the DE is operated in high voltage, there will be voltage induced strains [50]. These may result in premature failure of DE films. Furthermore, the *ripple* structures generate friction which may cause tearing and fatigue failure of the elastomer. We therefore incorporate factor of safety for the *ripple* design.

3.2. Prototype design

Following our analysis, we have made a 3D-printed prototype of the DEAmP generator. The device schematics is shown in Fig. 10a. We describe the cycle of operation in Fig. 5c, which suggests that the DEG must be charged when it is in its stretched state ($C_D = C_{D\_MAX}$) and be discharged in its relaxed state ($C_D = C_{D\_MIN}$). Hence, for maximal output, the piezoelectric generator must be deformed when the DEG is stretched to its maximum capacitance, while a circuit breaker is needed to ensure open-circuit relaxation of the DE and subsequent connection to the drain resistor once the DE is fully relaxed. To achieve this the piezoelectric diaphragm (PZT) is placed at bottom side of the *ripple* compression structure, to make the compression simultaneous and integrated and a passive mechanical switch (Fig. 10b) was introduced so that it will be open during the DE deformation and closes once the DE is fully relaxed. Fig. 10b shows a picture of the assembled prototype and the PZT diaphragm.

A fifth order *ripple* structure of diameter 8 cm and maximum deformed height of 2 cm ($h_R/r = 0.5$) was used. Putting these values into Eq. (17), we obtain a capacitance ratio: $\beta = 10$. VHB 4905 is equal-biaxially prestretched about 2 times and secured on a 3D

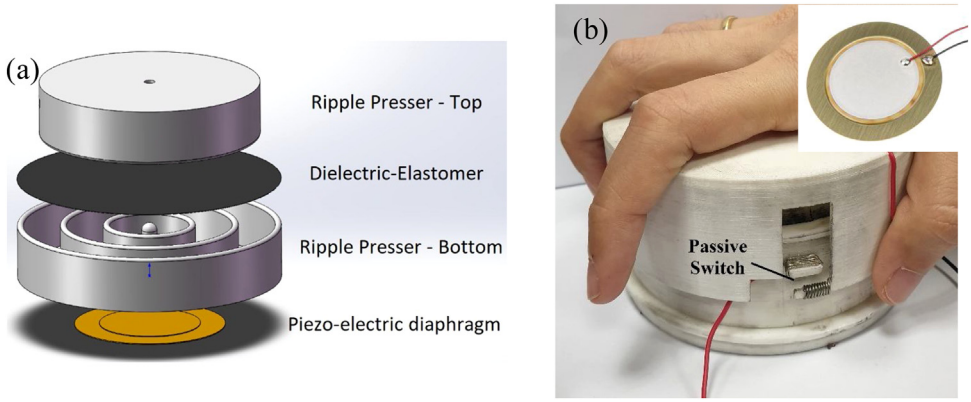

Fig. 10. Schematic of piezoelectric diaphragm–DEG coupled energy harvester: DEAmP. (b) Photograph of the prototype and the PZT diaphragm (top right).

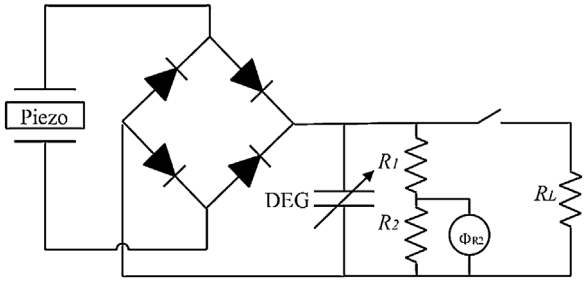

Fig. 11. Characterization circuit for conducting the experiments.

printed frame. Carbon grease is applied on both sides of the elastomer as the compliant electrodes. The *ripple* parameters (h_R/r and n) are represented in Fig. 9b. From Fig. 9a we can see that, the experimental parameters (h_R/r and n) lies below the rupture curve for $\lambda_p = 2$. Hence, we operate the elastomer in a safe zone. The PZT diaphragm we used has an active diameter of 20 mm and a thickness of 0.25 mm.

A circuit was made to compare the energy output of the piezoelectric generator and the piezo-DEG hybrid generator working under the same loading conditions (Fig. 11). High voltage IN4007 diodes are used for the full-wave bridge rectifier. A voltage divider (R_1 and R_2) was used to measure the voltage ($\Phi = \Phi_{R2}(R_1 + R_2)/R_2$). The value of R_1 and R_2 used in the experiments are 10GΩ and 10 MΩ respectively. A load resistor R_L is used to drain the charges from the DEG or the piezoelectric. Instantaneous power is (Φ^2/R_L) integrated with respect to time during the discharge phase of a cycle to find the energy output per cycle (Ω). Voltage data were captured using DAQ (NI USB-6356).

$$\Omega = \int_{t_1}^{t_2} \frac{\Phi^2}{R} dt \tag{21}$$

4. Experimental results for piezoelectric and DEAmP generators

To characterize the piezoelectric, the switch shown in Fig. 11 was closed and the DEG is electrically disconnected. The prototype is depressed to deform the piezoelectric. We show a typical discharge voltage profile for the piezoelectric generator in Fig. 12a. Fig. 12a corresponds to a drain resistor value of 10 MΩ. Reverse polarity during relaxation (as shown in Fig. 4b) was flipped by the signal rectifier (Fig. 11). We compute the output yield per cycle using Eq. (21). The output yield for five different values of resistances are investigated and plotted in Fig. 12b. Maximum energy yield was obtained when the drain resistor is 10 MΩ. Each data point was the average of 10 independent samples. The maximum output energy yield produced singly by a piezoelectric generator (Ω_{P_MAX}) is hence determined as 0.42 mJ.

The capacitance of the DEG prior to (C_{D_MIN}) and at maximum deformation (C_{D_MAX}) are measured to be 1.69 nF and 15.5 nF respectively ($\beta = 9.17$). Hence an error of 8.3% is found with the theoretical prediction of $\beta = 10$. The piezoelectric capacitance, C_P is measured to be nearly 20 nF ($C_{D\_MIN}/C_P = 0.085$). The capacitance measurements are made using a digital multimeter. The corresponding theoretical energy amplification calculated using Eq. (14) is 2.45 times. The same is indicated in Fig. 7 as dashed lines.

We identify four distinct processes in the operation of the hybrid DEAmP generator. In process I, the piezoelectric generator charges the DEG. In process II the DEG boosts the voltage. Processes I and II are done in an open-circuit condition, where the switch in Fig. 11

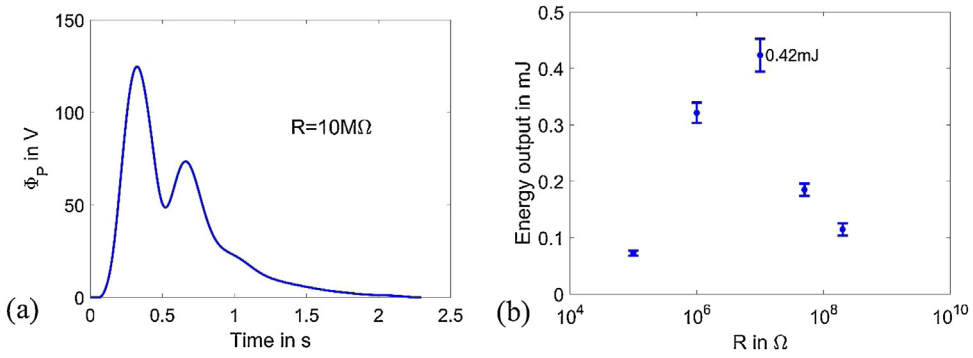

Fig. 12. (a) Voltage vs time plot for one cycle of the piezoelectric generator when the discharge resistance is, R_L is 10 MΩ. (b) Energy yield vs discharge resistance values (average and error bars for 10 experiments are shown).

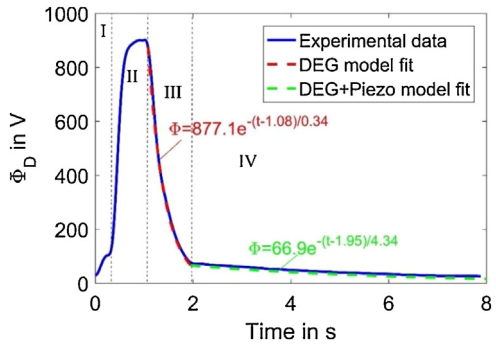

Fig. 13. Voltage vs time plot for the hybrid DEAmP generator.

is kept open. In process III, the boosted charges on the DEG are discharged through the load resistor and for process IV, the remaining energy on the piezoelectric capacitor (Ω_{P_r}) was discharged together with the DE. During processes III and IV, we kept the switch closed. We show a sample voltage vs time plot for the DEAmP generator in Fig. 13.

The discharge follows the capacitor discharge equation:

$$\Phi = \Phi_1 e^{\frac{t-t_1}{RC}} \tag{22}$$

Where $R = R_L = 200\,\text{M}\Omega$ and $C = C_{D\_MIN} = 1.69\,\text{nF}$. Φ_1 and t_1 are fitting parameters of experimental data. $\Phi_1 = 877.1\,\text{V}$ and $t_1 = 1.08\,\text{s}$. Eq. (22) was fit over the experimental data in Fig. 13 (fit shown in red). For process IV, the piezoelectric capacitor was discharged together with the DE. As DEG is connected in parallel to the piezoelectric, the effective capacitance is $C = 21.69\,\text{nF}$ ($C_P + C_{D\_MIN}$). The fit was plotted in Fig. 13 in green. The energy yield (Ω_{out}) was calculated using Eq. (21) for processes III and IV, giving an average value of 0.96 mJ for 10 cycles. The experimental energy amplification ($\Omega_{out}/\Omega_{P\_MAX}$) is hence calculated as 2.29 times (0.96 mJ/0.42 mJ). Our theory (Fig. 7) overestimates the actual amplification from our experiment by 7%. We attribute this to the dissipative losses in the DEG, piezoelectric and the electrical circuit.

The mass of the piezoelectric diaphragm (m_P) used in the prototype is measured to be 2.7 g. Using the density of VHB from datasheet (960 kg/m^3), the mass of the pre-stretched DE membrane used in the prototype (m_D) is calculated as 0.6 g. Hence the intrinsic specific energy output of the hybrid generator is found to be 0.29 mJ/g ($\Omega_{out}/(m_P+m_D)$). Note that the structural mass of the prototype is not included in this calculation. Similarly, the intrinsic specific energy of the piezoelectric diaphragm is calculated as 0.16 mJ/g (Ω_{P_MAX}/m_P). Hence, the coupling of piezoelectric generator with the DEG results in an intrinsic specific energy increase of 81%.

5. Discussion

To measure the efficiency of the prototype we connected it with a linear actuator (YAMAHA T9H10-250) as shown in Fig. 14a. A displacement profile similar to that of a hand press is applied by the linear actuator. A load cell (FUTEK LBS200) and a laser displacement sensor (KEYENCE IL300) are used to measure the force and displacement respectively. The force-displacement data of 10 cycles are shown in Fig. 14b. From the average area of a cycle, an average mechanical energy input (Ω_M) of 0.86 J was computed. The conversion efficiency is given by,

$$\eta = \frac{\Omega_{out}}{\Omega_M} \tag{23}$$

Eq. (23) gave us an efficiency number of about 0.11% for our prototype. We note the very low efficiency of our experiment as compared with other works on DEG, which showed efficiencies of up to 30% [14]. To achieve efficiency figures of that order, the net energy output, Ω_{out} should be maximized, for a given input mechanical energy, Ω_M. Our prototype was designed to be mechanically stretched near to the rupture limit of the elastomer (as illustrated in Fig. 9a). Due to operation close to its maximum deformation range, mechanical viscous losses become significant. Energy is also lost due to the contact friction between the DE film and the ripple structures. These factors contribute to a high value of Ω_M. Furthermore, the peak operating voltage of DEG of around 900 V, with an estimated electric field of 7.2 MV/m, is nowhere close to the dielectric strength for VHB, found to be around 250 MV/m [20]. Consequently, charge leakage may not be as significant as it is when subject to higher fields [51], and the electrical output may not be optimized at such a low electric field [18,52].The latter gave rise to a low value of Ω_{out}. As Ω_M is about 900 times higher than Ω_{out}, the low value of efficiency could reasonably be attributed to the large viscoelastic loss of VHB [53–55] and perhaps, some friction losses within the ripple structure. An elastomer with lower viscoelasticity may increase the efficiency significantly.

There are several ways by which the energy amplification ($\Omega_{out}/\Omega_{P\_MAX}$) may be improved. Fig. 15 shows the triangular DEG cycle used in our analysis. The yellow triangular area represents the input energy transferred to the DEG by the piezoelectric, Ω_{D_in} (Eq. 9a). For a given capacitance ratio (β) of the DEG, Ω_{D_in} is determined by . From Eq. (15) and Fig. 7b the optimal value of γ may be determined. Fig. 7b shows that the γ used in our prototype is much lower than the analytical optimal value. For a given C_P, γ ($= C_{D\_MIN}/C_P$) may be increased via a larger C_{D_MIN}. Using multilayers of DE membrane or using an elastomer with a higher permittivity and/or lower thickness will produce a larger C_{D_MIN}.

The green area in Fig. 15 shows the increase in electrical energy due to voltage amplification of DEG. For a given input energy, Ω_{D_in} the magnitude of this area is proportional to β. Fig. 7a suggests that

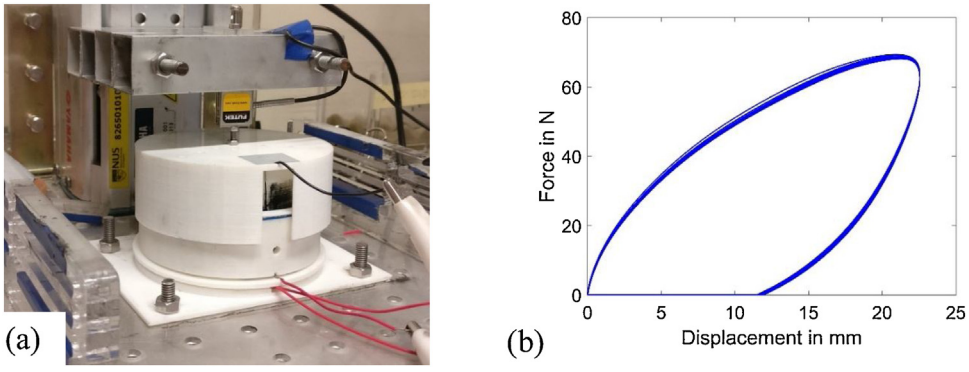

Fig. 14. (a) Characterization setup to find the mechanical input. (b) Force-displacement data for 10 DEAmP cycles.

Table 1
DEG performance when tethered to various priming sources.

Priming Source	Specific energy (mJ/g)	Mechanical-to-electrical conversion efficiency	Capacitance ratio (β)	Remarks
High Voltage Electrical Source [14]	780	30%	~57	Equal-biaxial stretching of DEG with an input voltage of 3 kV.
Electret [23]	0.55	Not mentioned	2.25	Electret material charged to ~1000 V.
Microbial fuel cell or solar cell arrays with self-priming circuit [28]	10	12%	Not specified	More than 30 cycles to boost the voltage from 10 V to a peak of 2000 V. Mechanical viscous loss is not considered in efficiency calculation.
Piezoelectric by Alexandru et al. [29]	0.285/cycle	Not mentioned	1.9	Bias voltage of 1 kV from piezoelectric. Application limited to sources that can provide compression to piezoelectric and uniaxial strain to DEG. Mass of the piezoelectric was not considered for the specific energy calculation.
Piezoelectric by Lamgomarsini et al. [30]	0.014	Not mentioned	2.2	Unclear if energy is indeed amplified by DEG.
Piezoelectric DEAmP (This work)	0.29	0.11%	9.2	Theoretical energy amplification of up to 250 times. Experimental value of 2.26 for a small-scale prototype. Specific energy increase of 81%.

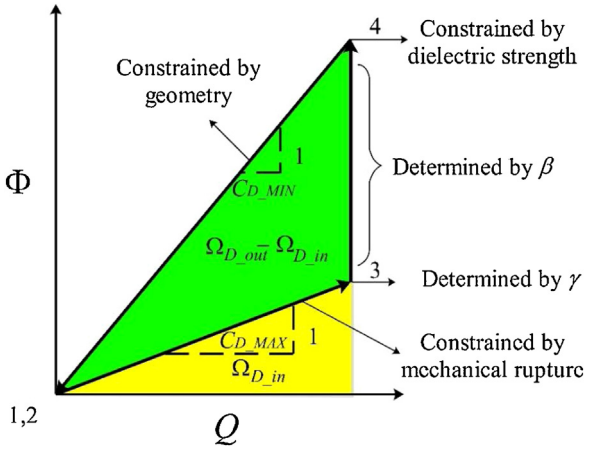

Fig. 15. The triangular cycle of DEG.

for $\beta \tilde{6}25$, the energy amplification attains a high of 250. Practically this is challenging to achieve due to limits of mechanical rupture, electric breakdown, loss of tension and electromechanical instability [17,43,47]. Material imperfections exacerbate material failure, which further limits the size of the triangular DEG cycle. Particularly, state 4 of the cycle is constrained by the dielectric strength of the elastomer, which is a highly variable property that is dependent upon factors like elastomer thickness and state of deformation [17,43,56]. Fig. 15 summarizes practical constrains on a DEG that limit energy amplification.

Table 1 compares several performance metrics for a DEG tethered to various priming sources. The specific energy output from our experiment (0.29 mJ/g) is much lower compared with the highest specific energy output of a DEG reported for an equal-biaxial DEG with a high voltage power supply (780 mJ/g) [14], but comparable with DEGs primed by electrets and piezoelectrics from other works. The significant gap between performances of DEG primed by piezoelectrics/electrets and other high voltage sources is the relatively small amount of energy transferred from the piezoelectric diaphragm. To increase the input energy from the piezoelectric priming source, one may try and deform the piezoelectric generator to enhance output energy to the DEG, for instance, subjecting the piezoelectric to an impulsive free-vibration. Piezoelectric materials with higher electromechanical coupling constants may also be used. Recent investigations into triboelectric nanogenerators (TENGs) that exploits contact electrification produced significant output power flux of 50 mW/cm^2 [57–60], which could serve as an excellent candidate to prime the DEG. Using multiple elements of such priming sources will also enhance the transferred energy. In this work we only focus on the energy amplification for a given priming source, and shall leave the study of priming source optimization and other priming sources out.

6. Conclusion

We have demonstrated, under non-optimized conditions, that a net specific energy gain of 81% was observed in a DEAmP system, as compared with a purely piezoelectric system. For a DEAmP to produce a net gain in output energy, the voltage boost across the DE must be sufficiently high. Using an analytical model, we proposed conditions of operation where a net gain for the hybrid generator is obtained and expressed it as a design plot. Analysis suggest that under optimal conditions, up to 250 times in amplification of output energy could be produced for a DEAmP compared to a stand-alone piezoelectric generator.

We proposed a *ripple* mode of deformation to effect significant capacitance change within a given constrained space. Such a method would greatly multiply the output performance of a DEG. Assuming homogeneous deformation, we created a design plot to select the parameters for the construction of the *ripple* configuration.

The energy amplification framework we presented in this work need not be limited to a diaphragm-type PZT material priming a *ripple*-type DEG. The priming source could be piezoelectric generators of a different material and geometry, it could be a triboelectric generator (TENG), or an electret. Our framework only requires the amount of output energy from the priming source transferred as input energy to the DEG, and the capacitance change ratio of the DEG, in order to estimate the net energy amplification due to the DEG and the conditions at which we can expect a net gain in output energy.

Declarations of interest

None.

Acknowledgements

This research was supported through funding from the 1st grant call under the Joint Science and Technology Research Cooperation between the Department of Science & Technology (DST), Govt. of India and the Agency for Science, Technology and Research (A*STAR), and from the NUS MOE strategic grant for Composites Engineering and Research. SJAK wishes to acknowl-

edge the A*STAR-DST grant no. R-265-000-524-305 (SERC 142 520 3140) for funding this research. Anup Teejo Mathew wishes to acknowledge the NUS Research Scholarship for PhD study in NUS from August 2015 to August 2019. Financial support for Liu Chong from NUS MOE strategic grant R-265-000-523-646 is gratefully acknowledged.

References

[1] S. Roundy, On the effectiveness of vibration-based energy harvesting, J. Intell. Mater. Syst. Struct. 16 (2005) 809–823, http://dx.doi.org/10.1177/1045389x05054042.
[2] J.A. Paradiso, T. Starner, Energy scavenging for mobile and wireless electronics, IEEE Pervasive Comput. 4 (2005) 18–27, http://dx.doi.org/10.1109/MPRV.2005.9.
[3] X. Wang, Chapter 11 - Ocean wave energy conversion analysis., in: X. Wang (Ed.), Frequency Analysis of Vibration Energy Harvesting Systems, Academic Press, 2016, pp. 249–269, http://dx.doi.org/10.1016/B978-0-12-802321-1.00011-X.
[4] W.S. Hwang, J.H. Ahn, S.Y. Jeong, H.J. Jung, S.K. Hong, J.Y. Choi, et al., Design of piezoelectric ocean-wave energy harvester using sway movement, Sens. Actuators A Phys. 260 (2017) 191–197, http://dx.doi.org/10.1016/j.sna.2017.04.026.
[5] R.D. Kornbluh, R. Pelrine, H. Prahlad, A. Wong-Foy, B. McCoy, S. Kim, et al., Dielectric elastomers: stretching the capabilities of energy harvesting, MRS Bull. 37 (2012) 246–253, http://dx.doi.org/10.1007/978-1-4614-5705-3_16.
[6] W. Yang, J. Chen, G. Zhu, J. Yang, P. Bai, Y. Su, et al., Harvesting energy from the natural vibration of human walking, ACS Nano 7 (2013) 11317–11324, http://dx.doi.org/10.1021/nn405175z.
[7] R.D. Kornbluh, R. Pelrine, Q. Pei, R. Heydt, S. Stanford, S. Oh, et al., Electroelastomers: applications of dielectric elastomer transducers for actuation, generation, and smart structures, SPIE's 9th Annual International Symposium on Smart Structures and Materials. International Society for Optics and Photonics (2002) 254–270, http://dx.doi.org/10.1117/12.475072.
[8] R. Pelrine, R.D. Kornbluh, J. Eckerle, P. Jeuck, S. Oh, Q. Pei, et al., Dielectric elastomers: generator mode fundamentals and applications, SPIE's 8th Annual International Symposium on Smart Structures and Materials. International Society for Optics and Photonics (2001) 148–156, http://dx.doi.org/10.1117/12.432640.
[9] H. Prahlad, R. Kornbluh, R. Pelrine, S. Stanford, J. Eckerle, S. Oh, Polymer power: dielectric elastomers and their applications in distributed actuation and power generation, in: Proceedings of ISSS, 2005, pp. 100–107 https://www.researchgate.net/publication/281535535_Polymer_power_Dielectric_elastomers_and_their_applications_in_distributed_actuation_and_power_generation.
[10] S. Chiba, M. Waki, T. Wada, Y. Hirakawa, K. Masuda, T. Ikoma, Consistent ocean wave energy harvesting using electroactive polymer (dielectric elastomer) artificial muscle generators, Appl. Energy 104 (2013) 497–502, http://dx.doi.org/10.1016/j.apenergy.2012.10.052.
[11] Z. Suo, Theory of dielectric elastomers, Acta Mech. Solida Sin. 23 (2010) 549–578, http://dx.doi.org/10.1016/S0894-9166(11)60004-9.
[12] R. Pelrine, High-speed electrically actuated elastomers with strain greater than 100%, Science 287 (2000) 836–839, http://dx.doi.org/10.1126/science.287.5454.836.
[13] R.D. Kornbluh, R. Pelrine, Q. Pei, S. Oh, J. Joseph, Ultrahigh strain response of field-actuated elastomeric polymers, SPIE's 7th Annual International Symposium on Smart Structures and Materials. SPIE (2000) 14, http://dx.doi.org/10.1117/12.387763.
[14] S. Shian, J. Huang, S. Zhu, D.R. Clarke, Optimizing the electrical energy conversion cycle of dielectric elastomer generators, Adv Mater. 26 (2014) 6617–6621, http://dx.doi.org/10.1002/adma.201402291.
[15] G. Moretti, P. Rosati Papini Gastone, L. Daniele, D. Forehand, D. Ingram, R. Vertechy, et al., Modelling and testing of a wave energy converter based on dielectric elastomer generators, Proc. R. Soc. A Math. Phys. Eng. Sci. 475 (2019), 20180566, http://dx.doi.org/10.1098/rspa.2018.0566.
[16] M. Giacomo, P. Gastone Pietro Rosati, R. Michele, F. David, I. David, V. Rocco, et al., Resonant wave energy harvester based on dielectric elastomer generator, Smart Mater. Struct. (2018), http://dx.doi.org/10.1088/1361-665X/aaab1e.
[17] S.J.A. Koh, X. Zhao, Z. Suo, Maximal energy that can be converted by a dielectric elastomer generator, Appl. Phys. Lett. 94 (2009), 262902, http://dx.doi.org/10.1063/1.3167773.
[18] S.J.A. Koh, C. Keplinger, T. Li, S. Bauer, Z. Suo, Dielectric elastomer generators: how much energy can be converted? IEEE/ASME Trans. Mechatron. 16 (2011) 33–41, http://dx.doi.org/10.1109/TMECH.2010.2089635.
[19] J. Huang, S. Shian, Z. Suo, D.R. Clarke, Maximizing the energy density of dielectric elastomer generators using equi-biaxial loading, Adv. Funct. Mater. 23 (2013) 5056–5061, http://dx.doi.org/10.1002/adfm.201300402.
[20] R. Kaltseis, C. Keplinger, S.J.A. Koh, R. Baumgartner, Y.F. Goh, W.H. Ng, et al., Natural rubber for sustainable high-power electrical energy generation, RSC Adv. 4 (2014) 27905–27913, http://dx.doi.org/10.1039/C4RA03090G.
[21] C. Jean-Mistral, T. Vu Cong, A. Sylvestre, Advances for dielectric elastomer generators: replacement of high voltage supply by electret, Appl. Phys. Lett. 101 (2012), 162901, http://dx.doi.org/10.1063/1.4761949.
[22] T. Vu-Cong, C. Jean-Mistral, A. Sylvestre, Y. BAR-COHEN, Autonomous dielectric elastomer generator using electret, Proc SPIE (2013) 86870H, http://dx.doi.org/10.1117/12.2008793.
[23] T. Vu-Cong, C. Jean-Mistral, A. Sylvestre, Electrets substituting external bias voltage in dielectric elastomer generators: application to human motion, Smart Mater. Struct. 22 (2013), 025012, http://dx.doi.org/10.1088/0964-1726/22/2/025012.
[24] C. Lagomarsini, C. Jean-Mistral, S. Monfray, A. Sylvestre, New approach to improve the energy density of hybrid electret-dielectric elastomer generators, in: SPIE Smart Structures and Materials+ Nondestructive Evaluation and Health Monitoring. International Society for Optics and Photonics, 2017, pp. 101632C-C-8.
[25] I.A. Anderson, I. Ieropoulos, T. McKay, B. O'Brien, C. Melhuish, A hybrid microbial dielectric elastomer generator for autonomous robots, SPIE Smart Structures and Materials+ Nondestructive Evaluation and Health Monitoring. International Society for Optics and Photonics (2010), http://dx.doi.org/10.1117/12.847379, pp. 76421Y-Y-11.
[26] I.A. Anderson, I.A. Ieropoulos, T. McKay, B. O'Brien, C. Melhuish, Power for robotic artificial muscles, IEEE/ASME Trans. Mechatron. 16 (2011) 107–111, http://dx.doi.org/10.1109/TMECH.2010.2090894.
[27] T. McKay, B. O'Brien, E. Calius, I. Anderson, Self-priming dielectric elastomer generator design, SPIE smart structures and materials + nondestructive evaluation and health monitoring. SPIE (2012) 9, http://dx.doi.org/10.1117/12.915464.
[28] T.G. McKay, B.M. O'Brien, E.P. Calius, I.A. Anderson, Soft generators using dielectric elastomers, Appl. Phys. Lett. 98 (2011), 142903, http://dx.doi.org/10.1063/1.3572338.
[29] C. Alexandru, C. Pierre-Jean, P. Lionel, Hybrid energy harvesting systems, using piezoelectric elements and dielectric polymers, Smart Mater. Struct. 25 (2016), 095048, http://dx.doi.org/10.1088/0964-1726/25/9/095048.
[30] L. Clara, J.-M. Claire, L. Giulia, S. Alain, Hybrid piezoelectric - electrostatic generators for wearable energy harvesting applications, Smart Mater. Struct. (2018), http://dx.doi.org/10.1088/1361-665X/aaf34e.
[31] Z. Yang, S. Zhou, J. Zu, D. Inman, High-performance piezoelectric energy harvesters and their applications, Joule 2 (2018) 642–697, http://dx.doi.org/10.1016/j.joule.2018.03.011.
[32] A. Khaligh, P. Zeng, C. Zheng, Kinetic energy harvesting using piezoelectric and electromagnetic technologies—State of the art, IEEE Trans. Ind. Electron. 57 (2010) 850–860, http://dx.doi.org/10.1109/TIE.2009.2024652.
[33] Y.B. Jeon, R. Sood, Jh. Jeong, S.G. Kim, MEMS power generator with transverse mode thin film PZT, Sens. Actuators A Phys. 122 (2005) 16–22, http://dx.doi.org/10.1016/j.sna.2004.12.032.
[34] N. Kong, D.S. Ha, A. Erturk, D.J. Inman, Resistive impedance matching circuit for piezoelectric energy harvesting, J. Intell. Mater. Syst. Struct. 21 (2010) 1293–1302, http://dx.doi.org/10.1177/1045389x09357971.
[35] S. Sherrit, H.D. Wiederick, B.K. Mukherjee, M. Sayer, An accurate equivalent circuit for the unloaded piezoelectric vibrator in the thickness mode, J. Phys. D Appl. Phys. 30 (1997) 2354, http://dx.doi.org/10.1088/0022-3727/30/16/014.
[36] K. Jina, B.L. Grisso, J.K. Kim, H. Dong Sam, D.J. Inman, Electrical modeling of Piezoelectric ceramics for analysis and evaluation of sensory systems, in: 2008 IEEE Sensors Applications Symposium, 2008, pp. 122–127 https://ieeexplore.ieee.org/document/4472956/.
[37] S. Priya, Advances in energy harvesting using low profile piezoelectric transducers, J Electroceram. 19 (2007) 167–184, http://dx.doi.org/10.1007/s10832-007-9043-4.
[38] S. Priya, Modeling of electric energy harvesting using piezoelectric windmill, Appl. Phys. Lett. 87 (2005), 184101, http://dx.doi.org/10.1063/1.2119410.
[39] T.H. Ng, W.H. Liao, Sensitivity analysis and energy harvesting for a self-powered piezoelectric sensor, J. Intell. Mater. Syst. Struct. 16 (2005) 785–797, http://dx.doi.org/10.1177/1045389X05053151.
[40] C. Keawboonchuay, T.G. Engel, Electrical power generation characteristics of piezoelectric generator under quasi-static and dynamic stress conditions, IEEE Trans. Ultrason., Ferroelectr. Frequency Control. 50 (2003) 1377–1382, http://dx.doi.org/10.1109/TUFFC.2003.1244755.
[41] K. Tang, J. Kan, T. Peng, Z. Yang, G. Cheng, Power performance of circular piezoelectric diaphragm generators, Front. Mech. Eng. China 3 (2008) 434–440, http://dx.doi.org/10.1007/s11465-008-0069-3.
[42] T.-Q. Lu, Z.-G. Suo, Large conversion of energy in dielectric elastomers by electromechanical phase transition, Acta Mech. Sin. 28 (2012) 1106–1114, http://dx.doi.org/10.1007/s10409-012-0091-x.
[43] J.-S. Plante, S. Dubowsky, Large-scale failure modes of dielectric elastomer actuators, Int. J. Solids Struct. 43 (2006) 7727–7751, http://dx.doi.org/10.1016/j.ijsolstr.2006.03.026.
[44] I.A. Anderson, S. Rosset, T. McKay, H. Shea, Stack design for portable artificial muscle generators: is it dangerous to be short and fat? in: SPIE Smart Structures and Materials+ Nondestructive Evaluation and Health Monitoring. International Society for Optics and Photonics, 2014, pp. 90560Q-Q-8.
[45] H. Böse, E. Fuß, Novel dielectric elastomer sensors for compression load detection SPIE Smart Structures and Materials + Nondestructive Evaluation and Health Monitoring. SPIE (2014) 13, http://dx.doi.org/10.1117/12.2045133.
[46] Z. Suo, X. Zhao, W. Greene, A nonlinear field theory of deformable dielectrics, J. Mech. Phys. Solids 56 (2008) 467–486, http://dx.doi.org/10.1016/j.jmps.2007.05.021.
[47] A.T. Mathew, S.J.A. Koh, Operational limits of a non-homogeneous dielectric elastomer transducer, Int. J. Smart Nano Mater. (2017) 1–18, http://dx.doi.org/10.1080/19475411.2017.1421276.

[48] R.S. Rivlin, A.G. Thomas, Rupture of rubber. I. Characteristic energy for tearing, J. Polym. Sci. 10 (1953) 291–318, http://dx.doi.org/10.1002/pol.1953.120100303.
[49] M. Pharr, J.-Y. Sun, Z. Suo, Rupture of a highly stretchable acrylic dielectric elastomer, J. Appl. Phys. 111 (2012), 104114, http://dx.doi.org/10.1063/1.4721777.
[50] P. Zanini, J. Rossiter, M. Homer, Modelling the effect of actuator-like behavior in dielectric elastomer generators, Appl. Phys. Lett. 107 (2015), 153906, http://dx.doi.org/10.1063/1.4933315.
[51] T. Gisby, S. Xie, E. Calius, I. Anderson, Y. Bar-Cohen, Leakage current as a predictor of failure in dielectric elastomer actuators, Proc SPIE (2010), 764213, http://dx.doi.org/10.1117/12.847835.
[52] T. McKay, B. O'Brien, E. Calius, I. Anderson, An integrated, self-priming dielectric elastomer generator, Appl. Phys. Lett. 97 (2010), 062911, http://dx.doi.org/10.1063/1.3478468.
[53] L. Patrick, K. Gabor, W. Michael, Characterization of dielectric elastomer actuators based on a visco-hyperelastic film model, Smart Mater. Struct. 16 (2007) 477, http://dx.doi.org/10.1088/0964-1726/16/2/028.
[54] X. Zhao, S.J.A. Koh, Z. Suo, Nonequilibrium thermodynamics of dielectric elastomers, Int. J. Appl. Mech. 3 (2011) 203–217, http://dx.doi.org/10.1142/S1758825111000944.
[55] C. Chiang Foo, S. Cai, S. Jin Adrian Koh, S. Bauer, Z. Suo, Model of dissipative dielectric elastomers, J. Appl. Phys. 111 (2012), 034102, http://dx.doi.org/10.1063/1.3680878.
[56] J. Huang, S. Shian, R.M. Diebold, Z. Suo, D.R. Clarke, The thickness and stretch dependence of the electrical breakdown strength of an acrylic dielectric elastomer, Appl. Phys. Lett. 101 (2012), 122905, http://dx.doi.org/10.1063/1.4754549.
[57] F.-R. Fan, Z.-Q. Tian, Z. Lin Wang, Flexible triboelectric generator, Nano Energy 1 (2012) 328–334, http://dx.doi.org/10.1016/j.nanoen.2012.01.004.
[58] W.-S. Jung, M.-G. Kang, H.G. Moon, S.-H. Baek, S.-J. Yoon, Z.-L. Wang, et al., High output piezo/triboelectric hybrid generator, Sci. Rep. 5 (2015), https://doi.org/10.1038%2Fsrep09309.
[59] J. Chen, Z.L. Wang, Reviving vibration energy harvesting and self-powered sensing by a triboelectric nanogenerator, Joule (2017), http://dx.doi.org/10.1016/j.joule.2017.09.004.
[60] Y. Wang, Y. Yang, Z.L. Wang, Triboelectric nanogenerators as flexible power sources, Npj Flex. Electron. 1 (2017) 10, http://dx.doi.org/10.1038/s41528-017-0007-8.

Biographies

Anup Teejo MATHEW received his Bachelor of Technology (Honors) in Mechanical Engineering from Indian Institute of Technology, Hyderabad in 2015. He is currently pursuing a PhD degree under the supervision of A/Prof. Soo Jin Adrian Koh at the Department of Mechanical Engineering, National University of Singapore. His research interest includes analysis, design and development dielectric elastomer transducers.

Chong LIU received Bachelor of Engineering (Engineering Science) degree from National University of Singapore in 2016. He then worked as a research engineer at National University of Singapore in A/Prof. Soo Jin Adrian Koh's research group for 2 years. His research interest includes developing and optimizing energy harvest devices using dielectric elastomers.

Tian Yao Nicholas NG received his Bachelor of Engineering degree in Mechanical Engineering in 2018 from the National University of Singapore. He is currently working in the factory automation industry as an application sales engineer at Keyence Singapore. His research interests include energy harvesting through reusable energy and design of electrical systems in automation

Soo Jin Adrian KOH is an Assistant Professor at the Department of Mechanical Engineering, National University of Singapore (NUS). He received his PhD in Integrative Sciences & Engineering at NUS in 2008. He was a Post-Doctoral Fellow at the Harvard School of Engineering & Applied Sciences between 2008 and 2010. He has published more than 20 papers on topics ranging from electroactive polymers, soft robotics, energy harvesting, photonics and molecular modelling. His works are highly cited, with a current h-index of 13. His research interests are motion-based energy harvesting, soft robotics actuation and autonomous sensing of civil structures. He is an invited speaker, workshop lecturer and keynote speaker to notable conferences like the SPIE EAPAD, MRS Fall, ASME/IEEE and EuroEAP.